Materials & Design 225 (2023) 111432

Contents lists available at ScienceDirect

Materials & Design

journal homepage: www.elsevier.com/locate/matdes

Nanostructured zig-zag γ-Mo_2N thin films produced by glancing angle deposition for flexible symmetrical solid-state supercapacitors

Zecui Gao [a,b,*], Tengfei Zhang [a,*], Qimin Wang [a,c,*], Paul Heinz Mayrhofer [b]

[a] School of Electromechanical Engineering, Guangdong University of Technology, 510006 Guangzhou, China
[b] Institute of Materials Science and Technology, Technische Universität Wien, Getreidemarkt 9, 1060 Vienna, Austria
[c] Key Laboratory of Green Fabrication and Surface Technology of Advanced Metal Materials, Ministry of Education, Anhui University of Technology, 243000 Anhui Maanshan, China

HIGHLIGHTS

- Zig-zag structured porous γ-Mo_2N films were prepared by glancing angle sputtering.
- A solid-state symmetric zig-zag γ-Mo_2N supercapacitor device was produced.
- The device achieves both superior high energy density and power density.
- The device exhibits excellent cycling stability and desirable mechanical flexibility.
- The open porous nanostructure accelerates ion diffusion and electron transfer.

GRAPHICAL ABSTRACT

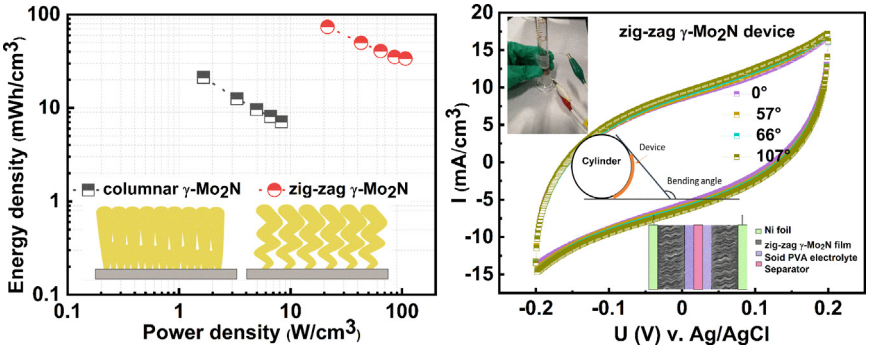

ARTICLE INFO

Article history:
Received 14 July 2022
Revised 21 November 2022
Accepted 24 November 2022
Available online 25 November 2022

Keywords:
γ-Mo_2N films
Glancing angle deposition
Flexible symmetric supercapacitor
Solid-state electrolyte

ABSTRACT

The performance of electrochemical capacitors strongly depends on their accessible surface area, chemical stability, and electrical conductivity. Simple columnar and zig-zag γ-Mo_2N thin-film electrodes were prepared by magnetron sputtering. The latter is obtained by glancing angle deposition (GLAD), which is known for open porous structures due to the ballistic shadowing effect. As intended, the zig-zag structured γ-Mo_2N electrode presents an outstanding area capacitance of 248 mF/cm^2 at a scan speed of 50 mV/s, which is 4 times higher than that of the simple columnar one. Both of them exhibit excellent cycling stability of 95 % over 20,000 cycles (at 200 mV/s). The symmetrical solid-state supercapacitor prepared with the zig-zag structured γ-Mo_2N thin film delivers an excellent power density of 107.1 W/cm^3 at 33.8 mWh/cm^3, and its volumetric capacitance is ~ 3.5 times higher than the simple columnar structured γ-Mo_2N device. Bending tests of such solid-state γ-Mo_2N supercapacitors proved their mechanical flexibility to a bending angel of even 107°. Based on these studies we can conclude that the highly porous zig-zag structured γ-Mo_2N-based electrodes prepared by GLAD combine outstanding electrochemical energy storage capabilities with excellent mechanical flexibility.

1. Introduction

Used as energy storage devices, supercapacitors (SCs) have the merits of high-power density, fast charge and discharge, long service life and safety [1,2]. Furthermore, they provide repairability

* Corresponding authors.
E-mail addresses: zecui.gao@tuwien.ac.at (Z. Gao), tfzhang@gdut.edu.cn (T. Zhang), qmwang@gdut.edu.cn (Q. Wang).

https://doi.org/10.1016/j.matdes.2022.111432
0264-1275/

[3], stretchability [4], and wearability [5], enabling them to meet the increasing requirements of commercial applications in flexible electronics. The energy storage properties of SCs are determined mainly by their composition and properties of the electrode materials, like porosity, wettability, conductivity, stability and redox properties. According to the charge storage mechanism, one of the main kind of electrochemical capacitors (ECs) are electrostatic double-layer capacitors (EDLCs), which, close to traditional capacitors, achieve the electrostatic storage of the electrical energy by separation of charge in a Helmholtz double layer at the interface between the surface of a conductive electrode and an electrolyte [4,6,7]. The most common examples are carbon-based materials, including carbon nanotubes [8] and graphene [9]. The other kind of ECs are pseudocapacitors, which, more like batteries, electrochemically store electrical energy by Faraday electron charge transfer with redox reactions, intercalation, or electro-sorption. Common examples are transition metal oxides [10], conducting polymers [11,12], and composite electrodes (such as vanadium nitride @ carbon nanobelts [13]). Since the amount of charge stored per unit voltage in a supercapacitor is predominantly attributed to multiple faradaic and non-faradaic reactions occurring at or near the electrode surface, the electrodes are typically as porous as possible (e.g., nanofiber structures) [14,15].

Recently, transition metal nitride (TMN) thin films (such as TiN [16], CrN [17–19], VN [20], HfN [21], and Mo_2N [12,22]) have attracted attention for SCs. The interest in these compounds is due to their excellent conductivity, high temperature and chemical stability, and high corrosion resistance, enabling a fast charge transfer and long-term service life of SC devices. Especially, the TMNs fabricated by physical vapour deposition (PVD), the most versatile and mature technology for TMNs, are famous for their high crystallinity, purity, and uniformity, as well as excellent substrate adhesion. Typically, the PVD process of TMNs was optimized to allow for dense growth morphologies, as these are needed prerequisites for improved diffusion barrier abilities, corrosion, mechanical and thermal stability, and superior mechanical strength [23]. However, for the application as SC materials, the TMN's should be very porous and rough [24], which can partly be obtained by limiting the adatom diffusion through lower deposition temperatures and higher deposition pressures [22]. Further possibilities to increase the porosity of TMNs are via a high-energetic Kr or Ar ion etching process (as shown for HfN [21]), or by selective leaching of a phase from the coating (as shown for CrN-Ni [25]). Another technique for preparing highly porous structures is glancing angle deposition (GLAD) in which the oblique angle of incidence flux during magnetron sputtering results in atomic shadowing effects [26,27]. Thereby, porous growth morphologies with single-tilted pillars or zig-zag tilted ones (when alternating the angle of incidence) are conveniently accessible. These unique morphologies lead to special mechanical, magnetic, and optical characteristics [28–30]. Here, we used GLAD to develop highly porous zig-zag tilted nanostructured γ-Mo_2N electrodes (shortly referred to as zig-zag) and compared them with simple columnar structured γ-Mo_2N electrodes (prepared by conventional magnetron sputtering).

Previous reports have highlighted the outstanding catalytic and electrical properties of γ-Mo_2N owing to its large specific surface area, rich intercalation chemistry, excellent chemical and thermal stability, and intrinsically high electrical and ionic conductivity [22,31–34]. In this work, we further amplify its charge storage capacity by systematically studying the electrochemical properties of the zig-zag γ-Mo_2N single electrode and its behavior in a flexible symmetric solid-state supercapacitor device. As envisioned, the zig-zag γ-Mo_2N electrode presents a 4 times higher specific capacitance than the simple columnar γ-Mo_2N electrode, without sacrificing long-term service life. Moreover, zig-zag symmetrical solid-state γ-Mo_2N supercapacitors also display outstanding volumetric capacitance, energy density and power density, and excellent mechanical flexibility.

2. Materials and methodology

2.1. Thin film deposition

Columnar γ-Mo_2N thin films were fabricated by sputtering a Mo target (99.99 % purity) in a mixed Ar/N_2 atmosphere utilizing a custom-built multifunctional physical vapor deposition instrument. The substrate materials were 100-oriented Si platelets ($10 \times 15 \times 0.5$ mm^3) and Ni foil (99.99 % purity), which were ultrasonically cleaned in acetone and ethanol for 30 min each. After reaching a base pressure below 5×10^{-3} Pa, an ion-assisted etching process was carried out in an Ar atmosphere with bias voltage of −600 V for 30 min to remove surface contaminants. The deposition time for the 2800-nm-thin columnar film was 3 h, while rotating the holder at 1.5 rpm (see the schematic, Fig. 1a). The zig-zag tilted microstructure was obtained by alternatingly tilting the sample holder between +36 and −36° (see the schematic, Fig. 1b). Thereby, we prepared a zig-zag coating with six stacks (three at +36° and three at −36°) – each for a deposition time of 30 min, resulting in six ∼ 467-nm-thin tilted stacks for a total thickness of ∼ 2800 nm. Both, the columnar and the zig-zag films were deposited with a discharge power of 2.0 kW, an Ar to N_2 flow rate ratio of 5:1, and a pressure of 0.7 Pa. The chamber temperature was kept constant at 250°C and the bias potential was set at −100 V.

2.2. Material characterization

Scanning electron microscopy (SEM, FEI Nova NanoSEM 430) was used to investigate the surface and cross-sectional morphologies of the columnar and zig-zag γ-Mo_2N films, at an accelerating voltage of 10 kV. At the same time, the integrated energy dispersive X-ray spectroscopy (EDX, Oxford instruments X-Max^N) system attached to the SEM, was used to detect their chemical compositions. An atomic force microscopy device (AFM, Bruker Dimension FastScan) was used to measure the surface morphology and root-mean-square roughness (R_q) of the films. The measurements were

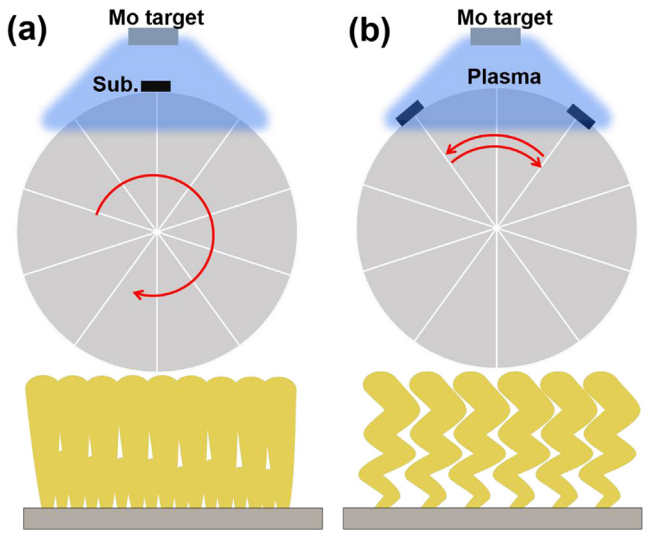

Fig. 1. Schematic sketch of the deposition procedure for **(a)** columnar and **(b)** zig-zag γ-Mo_2N films, using continuous rotation and alternating movement in front of the target (leading to a glancing angle deposition), respectively.

in peak force tapping mode and a dimension of 10 × 10 μm^2. The R_q was calculated from three consecutive measurements. X-ray diffraction (XRD, Bruker D8 Advance diffractometer) using a Cu Kα X-ray source (40 kV, 40 mA) in Bragg-Brentano configuration, was employed to examine the crystal structure of the films.

2.3. Electrochemical measurements

The electrochemical measurements presented in this work, including cyclic voltammetry (CV), galvanostatic charge–discharge (GCD), and electrochemical impedance spectroscopy (EIS), were systematically conducted on an electrochemical workstation (CHI660E, Shanghai Chenhua Corp.), in a 0.5 M H_2SO_4 aqueous electrolyte. For the straight columnar and the zig-zag γ-Mo_2N film electrodes, the electrochemical performance was evaluated using a conventional 3-electrode setup: the samples with a working area of 0.5 cm^2 as the working electrodes, an Ag/AgCl (sat. KCl) electrode as the reference electrode, and a Pt plate (20 × 20 × 0.5 m m^3) as the counter electrode. CV measurements were performed under 50–1000 mV/s, and GCD measurements were carried out at current densities of 1–10 mA/cm^2, with an open window potential of −0.2 to +0.2 V. EIS offers Bode and Nyquist plots, which can distinguish between pseudocapacitive, surface-controlled capacitive, and diffusion-limited faradaic mechanisms. EIS measurements were performed at frequencies range from 0.01 Hz to 100 kHz, at a potential perturbation of 5 mV.

For the symmetric flexible solid-state supercapacitor device (SSC), electrochemical properties were characterized in a two-electrode cell. 4 g PVA powder (alcoholysis degree: 99.4 %, Aladdin Chemicals) was put into 40 ml of 0.5 M H_2SO_4 solution (98 %, Analytical grade), and slowly and continuously stirred at 85°C for 2 h, until a transparent jelly-like solution was obtained. Two identical pieces of γ-Mo_2N films with a working area of 2.0 cm^2 (on Ni foil substrates) and a separator paper were soaked in the gel electrolyte for 30 min, and then dried under the ambient conditions for 10 min. After that, we sandwiched the separator paper with the two identical electrodes, and packaged them with a vacuum packaging machine to form a flexible symmetrical SSC device. The flexibility was tested by bonding the SSC devices on the surfaces of laboratory measuring cylinders with sizes of 100, 50 and 10 ml. Therefore, the bending angles are ~57, 66, and 107°, respectively, while the non-bonded device with an effective bonding angle of 0° acted as a reference.

2.4. Calculation

For the single electrodes, the area-specific capacitance (C_a, mF/cm^2) can be calculated based on the CV and GCD curves using the following equations [35], respectively:

$$C_a = \int I(U)dU/[2 \times v \times s \times \Delta U)] \quad (1)$$

$$C_a = I \times \Delta t/(s \times \Delta U) \quad (2)$$

where $\int IdU$ is the integrated area of a CV curve, at a certain potential sweep rate of v (mV/s), potential window ΔU (V), and electrode surface area s (cm^2). I (mA) and Δt (s) are the discharge current and time in a GCD curve, respectively.

For the symmetric solid-state supercapacitor device, cell-volumetric capacitance (C_{cell}, mF/cm^3) was derived also from both CV and GCD curves using the following equations, respectively:

$$C_{cell} = \int I(U)dU/[2 \times v \times V \times \Delta U)] \quad (3)$$

$$C_{cell} = (I \times \Delta t)/(V \times \Delta U) \quad (4)$$

The relative energy density (E, mWh/cm^3) and power density (P, W/cm^3) were calculated based on the following equations:

$$E = C_{cell} \times \Delta U^2/2 \times 3.6 \quad (5)$$

$$P = 3.6 \times E/\Delta t \quad (6)$$

where V (cm^3) represents the total volume of the two electrodes in a device.

3. Results and discussion

3.1. Structural characterization

SEM investigations of the samples prepared with a continuous substrate holder rotation are shown in Fig. 1a (top view) and Fig. 2c (cross-sectional), and with alternatingly reverting the sample holder between +36 and −36°are shown in Fig. 1b (top view) and Fig. 2d (cross-sectional). Fig. 2b clearly depicts a straight columnar structure, and Fig. 2d exhibits a zig-zag tilted structure. Both samples are ~2.8 μm thick and the zig-zag comprises six alternating stacks of ~467 nm each. The more detailed view into the zig-zag morphology, inset of Fig. 2b, clearly shows the separated and rough zig-zag pillars resulting from limited atomic reassembly kinetics and line-of-sight shadowing effects during GLAD [36]. The top-view morphology investigations of the thin films were also carried out by AFM, scanning over a surface area of 10 × 10 μm^2 for each sample, as shown in Fig. 3. AFM analysis is in line with the top-view SEM analysis that the zig-zag MoN has a rougher surface, yielding root mean square roughness (Rq) values of 23.2 and 39.3 nm for the columnar and zig-zag MoN thin-films, respectively.

The straight and zig-zag columnar samples deliver rough surface structures, see their top view SEM images in Fig. 2c and d, respectively. The surface of the zig-zag sample is even rougher and resembles a cauliflower structure, suggesting an improved specific area (beneficial for the charge absorption) compared to the straight columnar sample. XRD investigations suggest a face-centered cubic γ-Mo_2N structure (with the space group of *Pm*-3 m, ICDD 00–25-1366 [37]) for both samples, Fig. 4. This structure is characterized for γ-Mo_2N with only a half-occupied *N*-sublattice on which the vacancies are randomly distributed [38]. The most pronounced XRD peaks for both samples are at a diffraction angle of 37.4° suggesting a preferred (1 1 1) growth orientation. The zig-zag sample shows a broader full width at half maximum (FWHM), indicating smaller coherently diffracting domain sizes due to the alternating incidence angle of arrival species. According to Bragg's law and the position of these diffraction peaks, the lattice parameters of columnar and zig-zag γ-Mo_2N samples are 4.168 ± 0.015 and 4.186 ± 0.017 Å, respectively. The slightly larger lattice parameters of the zig-zag sample can be explained by its ~2.5 at.% higher nitrogen content than that of the columnar one, as shown in Table 1.

3.2. Electrochemical characterization of single electrode

The area-specific capacitances of the single columnar and zig-zag γ-Mo_2N electrodes were calculated in two ways: cyclic voltammetry (CV) and galvanostatic charge–discharge (GCD) curves – using Eqs. (1) and (2) – their results are given in Fig. 5a and 5d, respectively. The CV measurements were investigated under scanning rates of 100–1000 mV/s, and the GCD was performed using current densities from 1 to 10 mA/cm^2. As expected, regardless of the method, the area-specific capacitances of the zig-zag γ-Mo_2N electrode are ~ 4 times the value of the columnar electrode, when measured under the same conditions. With increasing scan

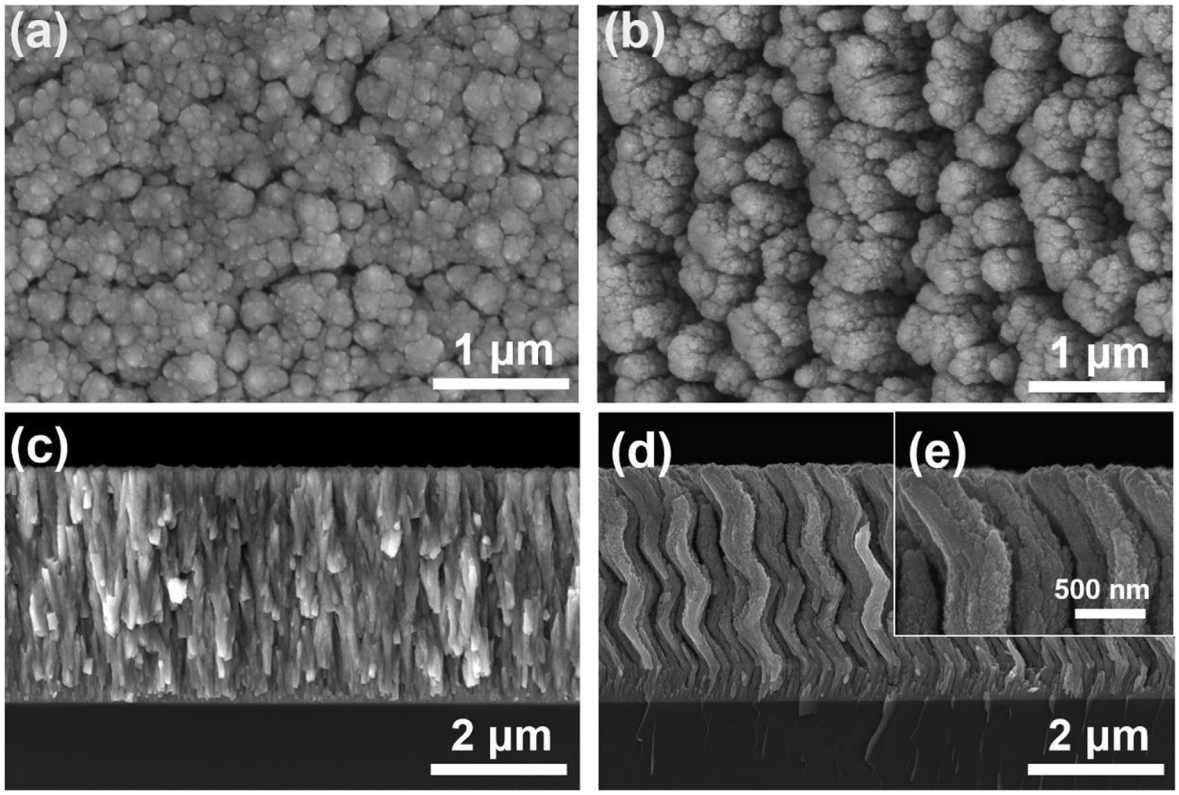

Fig. 2. Surface and cross-sectional SEM micrographs of **(a, b)** columnar and **(c, d)** zig-zag γ-Mo_2N films.

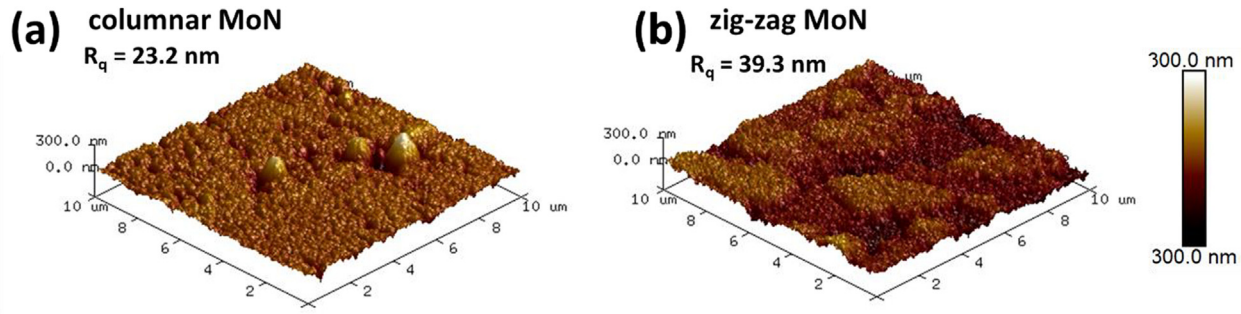

Fig. 3. AFM images of **(a)** columnar and **(b)** zig-zag γ-Mo_2N films.

rates and current densities, the specific capacitances of the zig-zag electrode decrease from 248.5 to 144.6 mF/cm^2 (from CV), and 195.7 to 77.2 mF/cm^2 (from GCD). The specific capacitance retention of the columnar film also decrease from 87.7 to 55.2 mF/cm^2 (from CV), and 62.4 to 22.8 mF/cm^2 (from GCD). Our zig-zag γ-Mo_2N electrode presents higher specific capacitances than most reported TMN film electrodes, such as porous CrN (58.5 mF/cm^2, at 1.0 mA/cm^2) [25] and nanotube TiN (69.05 mF/cm^2, at 0.3 mA/cm^2) [39]. The sputtered 16-μm-thick VN reached a super high specific capacitance of 1.2F/cm^2 (at 50 mV/s) [40], suggesting that the zig-zag γ-Mo_2N film electrode could further be improved by increasing the film thickness. Furthermore, even though the areal capacitances decrease as the scan rates increase, the zig-zag γ-Mo_2N still retains 144.6 mF/cm^2 at 1000 mV/s, which is facilitated by the rapid ion diffusion rate and electron transfer rate.

Fig. 5b and 5c show the CV curves of columnar and zig-zag γ-Mo_2N electrodes at scanning rates from 100 to 1000 mV/s, respectively. The improved specific capacitance of the zig-zag sample is clearly visible by comparing the integral areas under the CV curves (at the same scanning rate), since the capacitance is normalized to the geometric area of the CV curve. The quasi-rectangular shape of the cyclic voltammograms suggests an electrochemical storage mechanism similar to that of a Helmholtz double layer. The charge storage mechanism of γ-Mo_2N in H_2SO_4 aqueous solution relies on concurrent contributions from faradaic electrochemical storage of the active materials (H^+) and double-layer charging [41]. Obviously, the porous zig-zag structure offers more active adsorption sites for H^+ ions in 0.5 M H_2SO_4 solution, as well as a shorter diffusion length of electrons and ions, which gives a higher power density [41]. Therefore, the almost symmetrical rectangular CV curves exhibit remarkable rate performance and good reversibility of the electrodes, even at the high scanning rate of 1000 mV/s.

Analogically, the GCD curves of columnar and zig-zag γ-Mo_2N electrodes at current densities spanning from 1 to 10 mA/cm^2 are depicted in Fig. 5e and 5f, respectively. According to Eq. (2), the specific capacitance is only related to the discharging time of the GCD curves. For the same current densities, the longer the discharger time the higher is the specific capacitance. Thus, we can

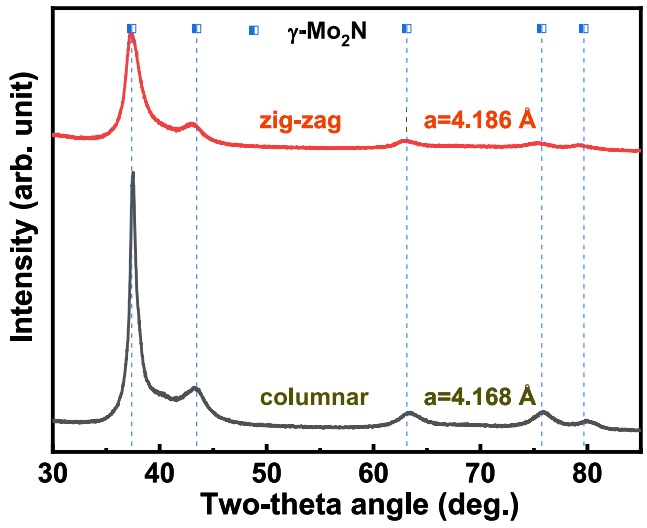

Fig. 4. XRD patterns of columnar and zig-zag γ-Mo_2N films.

Table 1
The chemical composition of the columnar and zig-zag MoN samples, provided by EDX spectra.

Element	columnar MoN at.%	zig-zag MoN at.%
N	34.67	36.44
Mo	65.33	63.56

easily tell that the zig-zag γ-Mo_2N electrode presents a strongly improved specific capacitance compared to the columnar films. Also, the almost equilateral-triangular GCD curves, as well as decent linear potential-time profiles, provide evidence for an EDLC mechanism (surface-controlled adsorption) storage mechanism and good reversibility of the electrodes. The high current density up to 10 mA/cm^2 displays remarkable rate performance. The utilization of the electrode surface is higher at high current densities [42]. This is because the zig-zag architecture provides a larger specific surface area and more active sites for charge storage, increasing the number of electrolyte ions entering the active material, shortening the diffusion length, and thus offering an extraordinary high supercapacitor performance.

EIS measurements were conducted to further disseminate the interfacial properties of the columnar and zig-zag thin film γ-Mo_2N electrode systems. Fig. 6a and 6b show Nyquist plots at frequencies of 0.01 to 100 kHz and 0.2 to 100 kHz, respectively. The corresponding simulation result of γ-Mo_2N, Fig. 6c, includes an ohmic resistance (R_s), a charge-transfer resistance (R_{ct}), a constant phase element (CPE), and a Warburg resistance (W). Their values could be determined by curve fitting simulation using Z-view software, or simply read from Fig. 6b. The R_s value is determined by the intersection between Nyquist curves and the horizontal axis in the ultrahigh frequency region, see Fig. 6b. Both electrode systems have roughly similar R_s values of ~1.6 Ω, indicating similar bulk solution resistance, intrinsic resistance of the active material, and interfacial contact resistance. The R_{ct} value can be estimated by deducing the diameter of the semicircle emerging in the high frequency region, see Fig. 6b. The zig-zag γ-Mo_2N electrode displays a semicircle diameter of ~2.26 Ω, while the columnar film only yields 0.48 Ω, leading to a dominance of the Warburg impedance at very low resistances of the columnar electrode. This can be ascribed to a better ohmic contact between the Mo_2N layer and Si current collector. In combination with the XRD results, this could be explained by a lower number of defects in the columnar γ-Mo_2N electrode. At high frequencies, the impedance of the capacitor will be very low and the major part of the current will flow through the capacitor. With decreasing frequencies from 100 kHz to 0.01 Hz, the impedance of the capacitor increases and a bigger fraction of the current flows through the resistor. When the majority of the current flows through the resistor, the total imaginary resistance Z'' will drop as the real part Z' increases. These processes lead to a semicircle in the Nyquist plot. Thus, the absence of semicircles in the high frequency range of the Nyquist plot of the columnar electrode also indicates low resistance values in the electronic charge transfer. The impedance of CPE, the Warburg diffusion impedance and the total electrochemical impedance of the equivalent circuit could be obtained using the formula in Ref. [39].

The Bode diagram (Fig. 6d) plots the phase shift (y-axis) as a function of the logarithmic scale of the frequency (x-axis). In the low frequency region, the phase angle reaches about −83° for both electrodes, presenting an excellent capacitive behavior. As marked with dotted horizontal lines in Fig. 6b, an ideal capacitor produces a slope of −90° and an ideal resistor yields 0°. The characteristic frequency (f_0) at the −45° phase angle denotes the crossover frequency of diffusive response, at which capacitive impedance equals the resistive impedance. Therefore, the corresponding characteristic time τ_0 ($\tau_0 = 1/2\pi f_0$) indicates the crossover time between capacitive and resistive behavior. The f_0 is ~1.21 and ~0.38 Hz and the τ_0 is 131.5 and 418.8 ms for the columnar and zig-zag γ-Mo_2N electrodes, respectively. Thus, the zig-zag electrode takes more time to change from resistive to capacitive processes. But in general, the extremely small τ_0 values strongly suggest an ultrafast-charging process.

The long-term cycling stabilities of the columnar and zig-zag γ-Mo_2N film electrodes were evaluated by CV cycles, at a sweep rate of 200 mV/s. The respective specific capacitance retentions during the CV cycles are plotted in Fig. 7a and 7b. Notably, both electrodes have excellent cycling stability, retaining 94.5 and 96.6% of the original capacitance after 20000 CV cycles, respectively. Such excellent cycling stability can be attributed to the chemical stability of the Mo_2N films, as well as the excellent adhesion between the film and the substrate facilitated by physical vapor deposition [43]. The stability is comparable to other TMN electrodes, such as TiN/Ni (98.22%/10000 GCD cycles) [44].

While the overall capacitance retention after 20000 cycles is similarly high for both film architectures, they show slightly different capacitance trends along the way: the specific capacitance of the columnar electrode drops noticeably in the first 1000 cycles, but remains stable afterwards. The zig-zag electrode on the other hand, falls slowly, but rises again after 16000 cycles. The capacitor recovery may be due to an electrochemical etching changing the surface topography [45]. The insets of Fig. 7b and 7d show CV curves of the first and last cycles of the columnar and zig-zag electrodes. After 20000 CV tests, their CV shapes are changed slightly, but are still rectangular.

3.3. Flexible symmetrical solid-state supercapacitors

In order to encourage the industrial application of γ-Mo_2N film supercapacitors, we assembled two flexible symmetrical solid-state devices from columnar and zig-zag γ-Mo_2N film electrodes, with a (0.5 M) H_2SO_4/PVA gel electrolyte. Their electrochemical performances were also evaluated by CV, GCD, and long-term CV cycling stability. Their volumetric capacitances were calculated form CV (Fig. 8a) and GCD (Fig. 8d) curves, using Eqs. (3) and (4), respectively. CV measurements were performed at scanning rates of 50–1000 mV/s (Fig. 8c and 8d), and GCD measurements under current densities from 1 to 5 mA/$cm^3$for the columnar device (Fig. 8e), and 1 to 10 mA/$cm^3$for the zig-zag device (Fig. 8f). As shown in Fig. 8a, with increasing scanning rates (from 50 to

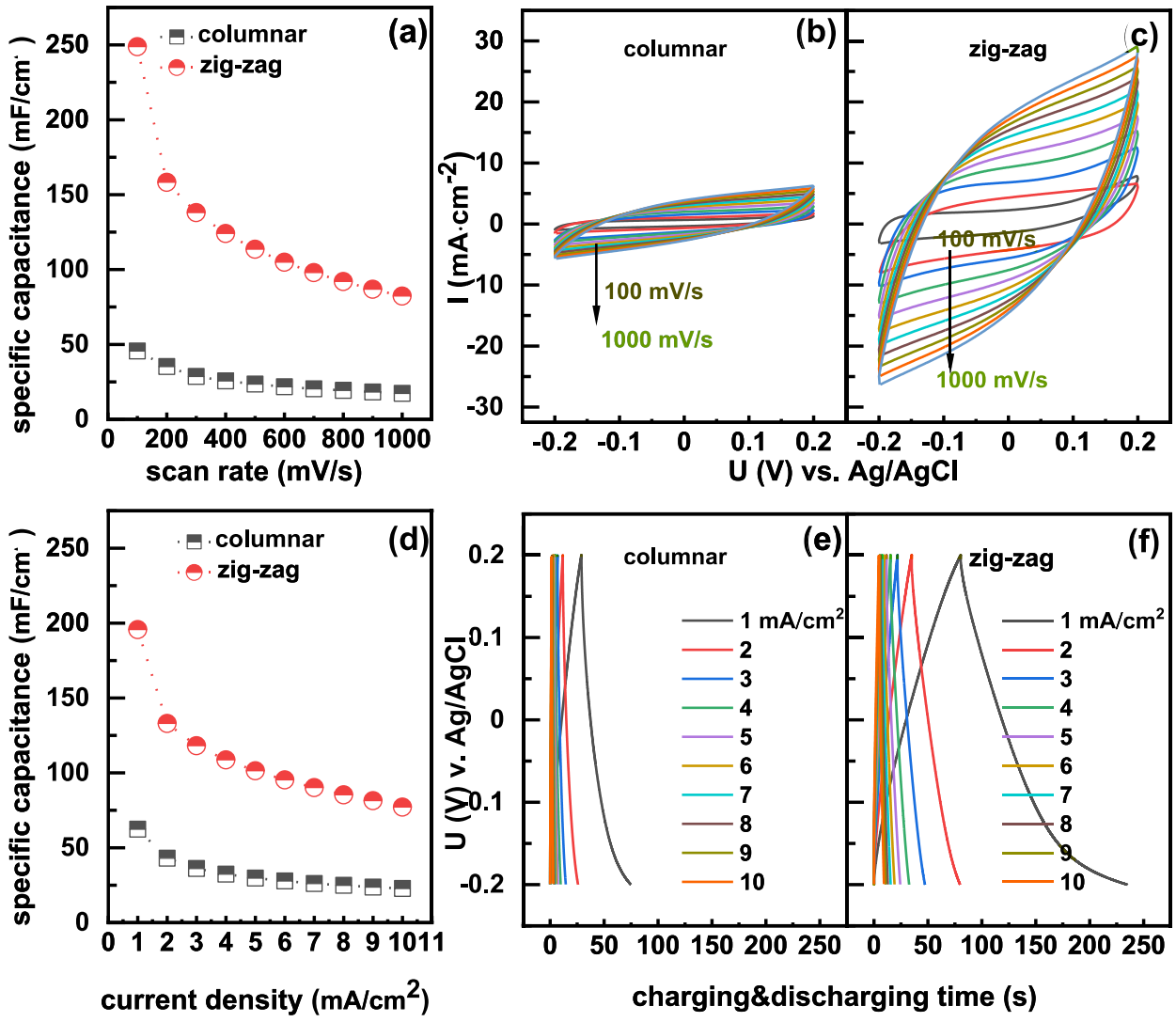

Fig. 5. (**a**) Area-specific capacitance, as a function of scan rate, calculated from the CV curves of (**b**) columnar and (**c**) zig-zag γ-Mo_2N film electrodes. (**d**) Area-specific capacitance, as a function of current densities, calculated from the GCD curves of (**e**) columnar and (**f**) zig-zag γ-Mo_2N film electrodes.

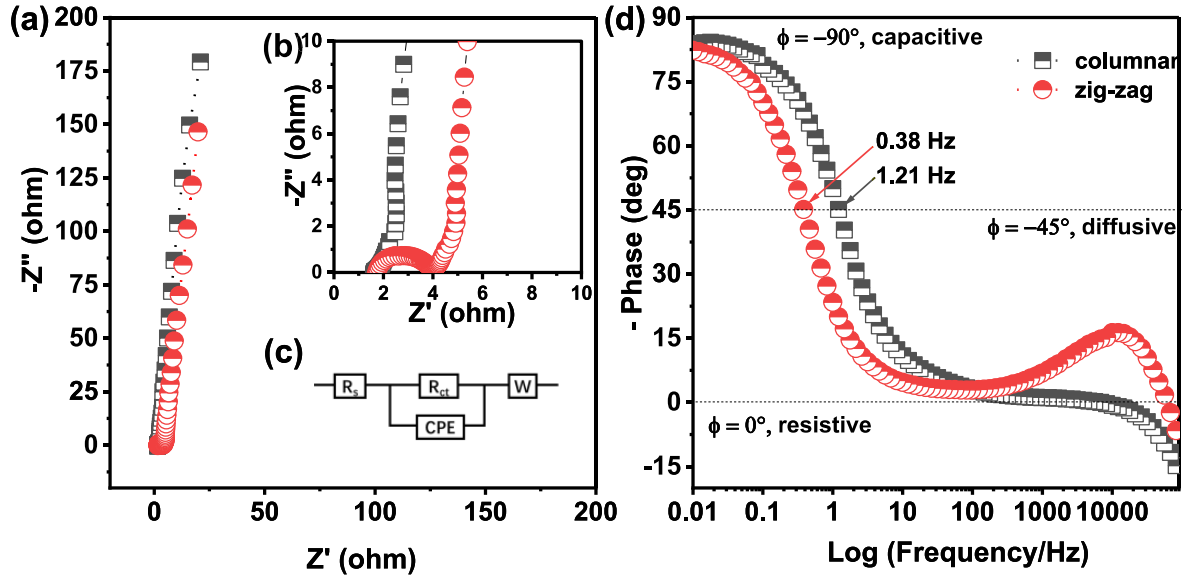

Fig. 6. EIS properties of the columnar and zig-zag γ-Mo_2N film electrodes: (**a**) Nyquist plots in the frequency region from 0.01 to 10 kHz, (**b**) Nyquist plots in the frequency region from 0.2 to 10 kHz (the high-frequency region), (**c**) the corresponding Randles circuit, and (**d**) Bode plots.

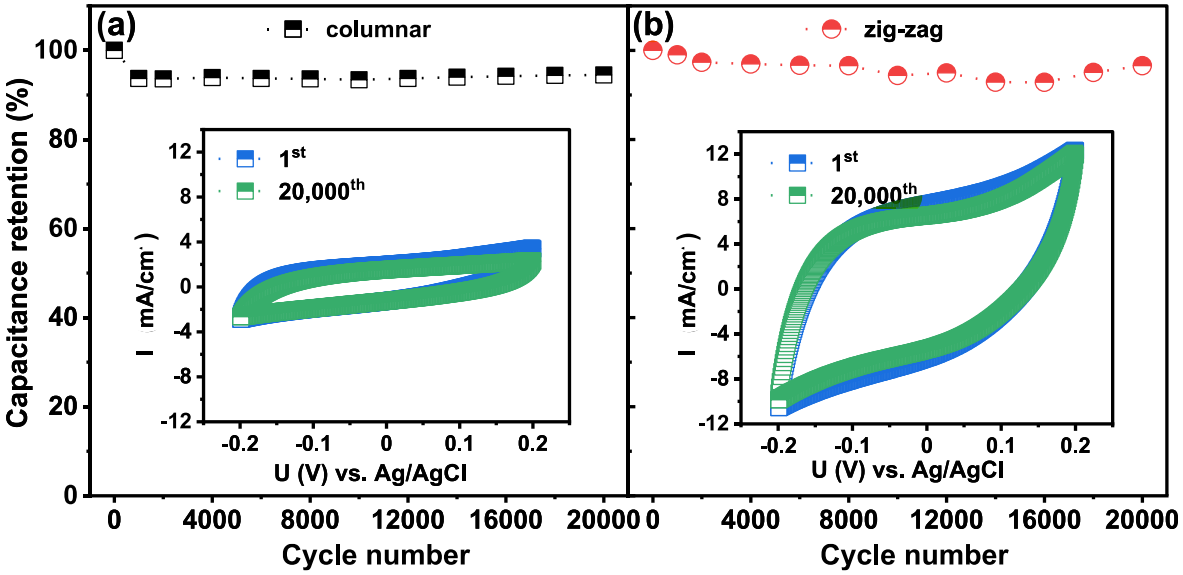

Fig. 7. Cycling performance of **(a)** columnar and **(b)** zig-zag γ-Mo_2N film electrodes. The insets show CV plots of the 1st and 20000th CV cycle (at 100 mV/s) of both electrodes, respectively.

1000 mV/s), the volumetric capacitance retention of the zig-zag device gradually decrease from 17.7 to 5.3 F/cm^3, and that of the columnar device drops from 6.1 to 2.2 F/cm^3. Similarly, as shown in Fig. 8c, with the current densities increasing, the capacitance retention of the zig-zag device gradually decrease from 19.9 to 5.3 F/cm^3 (at 1 – 10 mA/cm^3), and those of the columnar device drop from 5.7 to 1.9 F/cm^3 (at 1 – 5 mA/cm^3). The volumetric capacitance of the zig-zag device is also ~3.5 times that of the columnar device, which is also proven in single electrodes. Our zig-zag γ-Mo_2N device exhibits comparable volumetric capacitance to other supercapacitor devices, like the chrysanthemum-like TiN device (7.78 F/cm^3, at 0.05 mA/cm^3) [46], the CNT/MnO_2 hybrid SC (5.1 F/cm^3, at 16 mA/cm^3) [47], and the MnO_2/CNT/MoO_3/CNT asymmetric supercapacitor (4.9 F/cm^3, at 80 mA/cm^3) [48].

The rectangular characteristics of the CV curves of the columnar and zig-zag devices remain even up to 1000 mV/s, indicating typical double-layer capacitance performance and good reversibility. As predicted, the integral area of the CV curves of the zig-zag device is much larger than that of the columnar device, when compared at the same conditions. All the GCD curves remain nearly symmetrical with their discharging counterpart, while slightly non-linear potential-time profiles contribute to an increased resistance in the devices compared to the single electrodes. The discharge time of the zig-zag device is much longer than that of the columnar device, when compared at the same conditions. The current densities of the columnar device can reach only up to 5 mA/cm^3, which is caused by the insufficient time available for ion diffusion at higher current densities.

To test the cyclic stabilities of the columnar and zig-zag devices, they were subjected to 20000 CV circles at 100 mV/s. As shown in Fig. 9a and 9b, the capacitances of both devices decayed by approximately 13% (columnar) and 14% (zig-zag) after 20000 CV cycles. However, the capacitance of the columnar device remained stable first and declined rapidly after 15,000 cycles. That of the zig-zag device decreased within the first 10,000 cycles but then even increased slightly. The insets of Fig. 9a and 9b – showing the respective first and last CV cycles – exhibit no significant changes in the shapes of the first and last CV curves of the columnar and zig-zag devices, but their integrated area declines. Hence, the cycling performance of the devices is not as excellent as that of the single electrodes, but still comparable to the nanopyramids Mo_2N symmetric device (~89.93% retention after 4500 cycles) [22], and some other nitride-based and carbon-based solid-state (symmetric or asymmetric) supercapacitor devices listed in the supplementary information of reference [46].

To further evaluate the electrochemical performance of flexible symmetrical solid-state γ-Mo_2N supercapacitors, power and energy densities are calculated using Eqs. (5) and (6). As shown in Fig. 10a, the zig-zag device exhibits calculated volumetric energy densities of 49.8, 40.7, 35.1, 33.8 mWh/cm^3 and power densities of 42.9, 64.3, 85.7, 107.1 W/cm^3 at 1, 2, 3, 4, 5 mA/cm^2, respectively. These values are much higher than those of the columnar device (7.1 mWh/cm^3 and 8.2 W/cm^3, at 5 mA/cm^2) and even exceed other nitride-based symmetric supercapacitor devices (e.g., porous and non-porous CrN/CrN [17 18], as well as chrysanthemum-like TiN [46]). The improved electrochemical performance is a consequence of the zig-zag nanostructure providing abundant active sites and creating efficient uni-directional electron transfer pathways.

Recently, wearable electronics have elicited a continuously intensifying surge of interest. Therefore, we also investigated the flexibility of our nanostructured zig-zag symmetrical solid-state γ-Mo_2N film supercapacitor. The flexibility test was carried out by rolling the device onto laboratory measuring cylinders of various sizes (from 100 to 10 ml), to obtain gradually increasing bending angles from ~ 0 to 107°, see the schematic in Fig. 10b. All CV curves are almost overlapping at different bending angles, even at the highest bending angle of 107°, which demonstrates excellent flexibility and mechanical stability of the zig-zag device. The device only bent once before the electrochemical analysis, and the analysis was doing while bent. Such good flexibility is a direct result of the chemical stability of the Mo-N bonds and the excellent adhesion between film and substrate. This proves the possibility for further applications in wearable energy storage devices. However, still further work is needed in the evaluation of the electrode behavior after repetitive bending.

4. Conclusions

Zig-zag tilted-structured γ-Mo_2N films have been fabricated by glancing angle magnetron sputtering for supercapacitor electrodes.

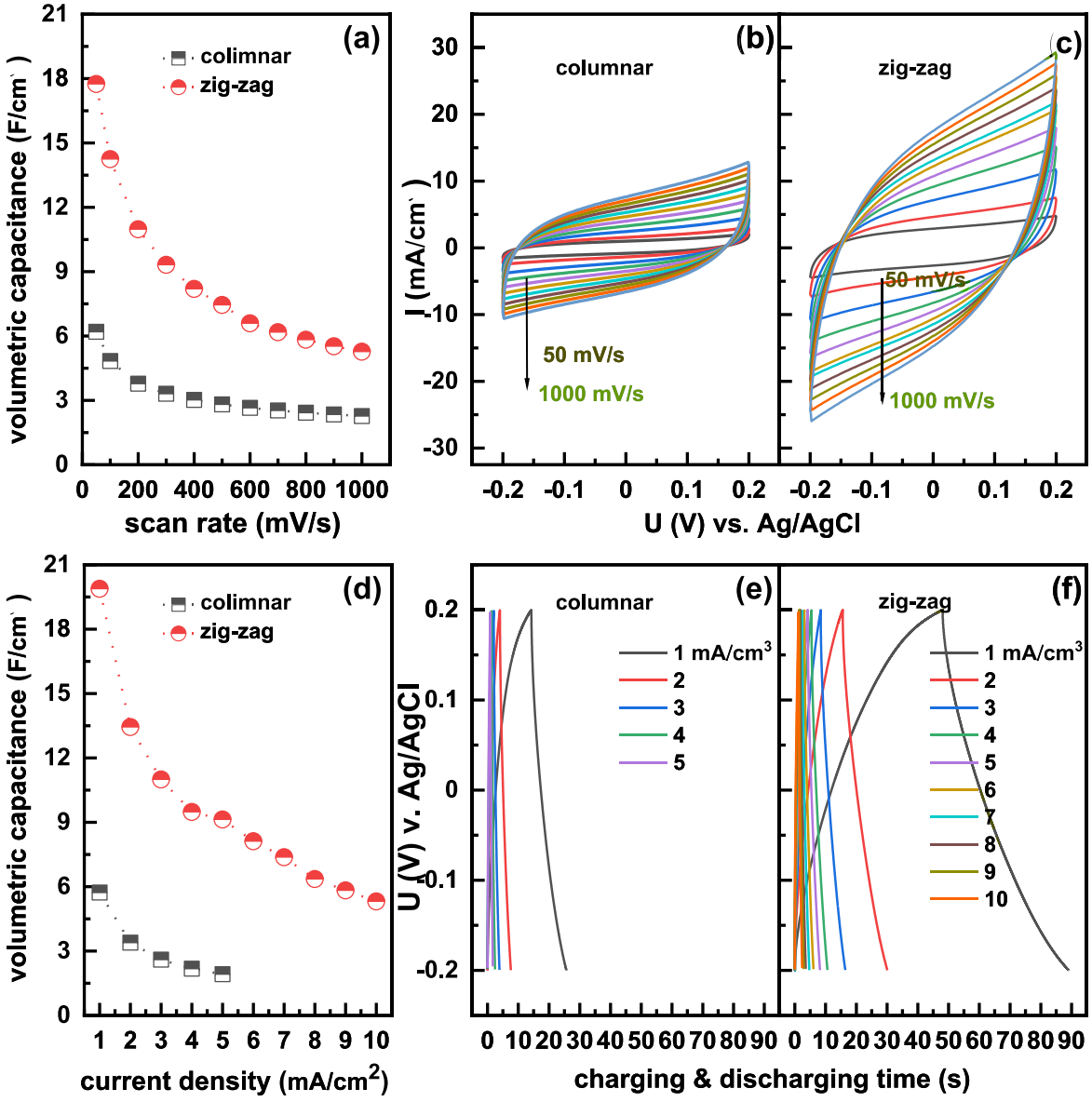

Fig. 8. **(a)** Volumetric capacitances as a function of scan rates calculated from the CV curves of **(b)** columnar and **(c)** zig-zag γ-Mo_2N devices. **(d)** Volumetric capacitances as a function of current densities calculated from the GCD curves of **(e)** columnar and **(f)** zig-zag γ-Mo_2N devices.

Compared to the conventional simple columnar-structured γ-Mo_2N electrode, the zig–zag electrode exhibits a 4 times higher area-specific capacitance of 248 mF/cm^2 (at a scan speed of 50 mV/s), without sacrificing cycling stability (96.5 % after 20000 CV cycles, at 200 mV/s). Furthermore, we successfully produced flexible symmetrical solid-state γ-Mo_2N supercapacitors with a 0.5 M H_2SO_4-PVA gel as electrolyte. The zig-zag SCs exhibit ultrafast charging/discharging capability, which yields an excellent volumetric capacitance of 19.9 F/cm^3 (at 1.0 mA/cm^3) with an extremely high energy density of 73.6 mWh/cm^3 at a power density of 21.4 W/cm^3. Moreover, the zig-zag SC shows a favorable cycling stability, retaining 85 % of the initial capacitance after 20000 CV cycles (at 200 mV/s). In addition, the symmetric zig-zag SCs also shows high mechanical flexibility, to be used for flexible devices. The excellent performance is based on the three-dimensional zig-zag architecture and the high conductivity and structural stability of the γ-Mo_2N films produced by magneton sputtering. Based on our results we can conclude that zig-zag γ-Mo_2N film electrodes prepared by glancing angle deposition provide ultrafast-charging/discharging abilities with excellent stability. They allow to prepare very flexible solid-state supercapacitors to be used for electrochemical energy storage and conversion applications.

Data availability

Data will be made available on request.

Declaration of Competing Interest

The authors declare that they have no known competing financial interests or personal relationships that could have appeared to influence the work reported in this paper.

Acknowledgements

The work was financially supported by the projects of National Key Research and Development Program of China (Grant No.

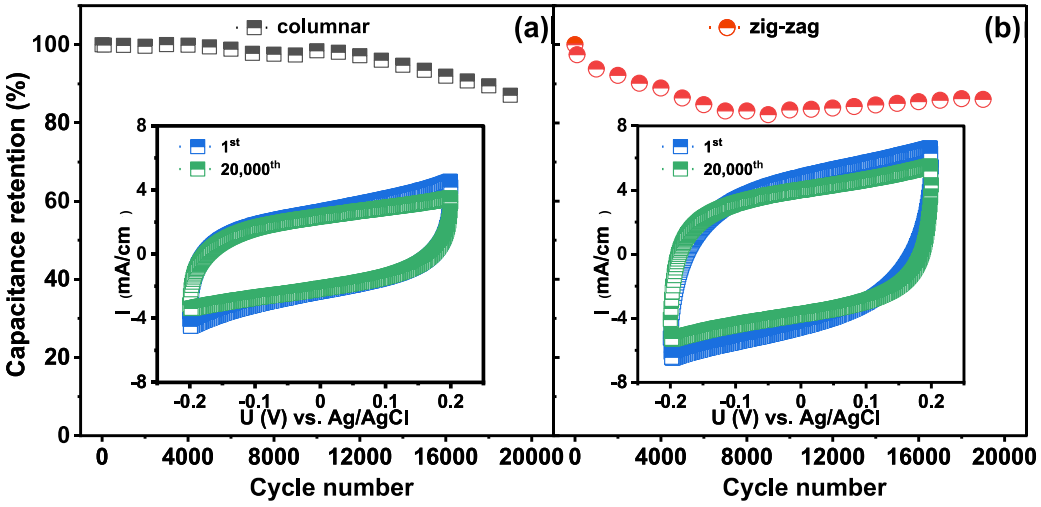

Fig. 9. Cycling performance of **(a)** columnar and **(b)** zig-zag γ-Mo_2N devices. The insets show the 1st and the 20000th CV cycle (at 200 mV/s) of columnar and zig-zag devices, respectively.

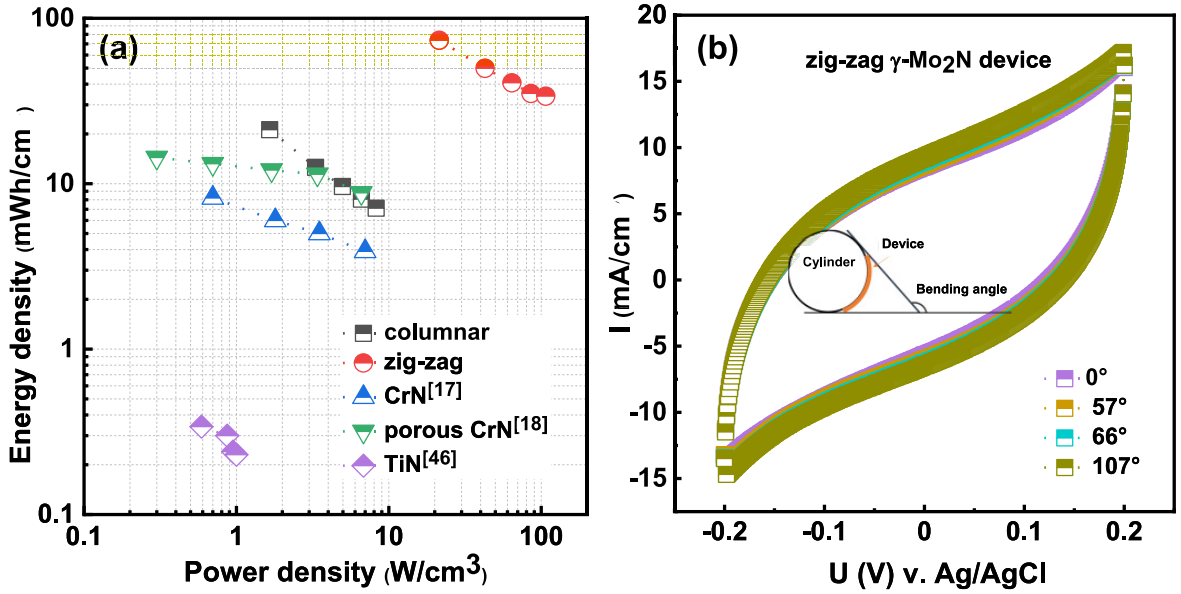

Fig. 10. **(a)** Energy and power densities of the symmetric γ-Mo_2N supercapacitors compared to some available energy storage systems. **(b)** CV curves of the zig-zag γ-Mo_2N device at different bending angles. The scan rate is 300 mV/s.

2017YFE0125400) and Natural Science Foundation of Guangdong Province of China (Grant No. 2020A1515010968). Zecui Gao thanks to the finical support of Chinese Scholarship Council during her PhD study time at TU Wien (No. 201908440933). The authors thank Dr. Julian Buchinger for the English revision. The authors acknowledge the TU Wien Bibliothek for the financial support through its Open Access Funding Program.

References

[1] Y. Zhou, W. Guo, T. Li, A review on transition metal nitrides as electrode materials for supercapacitors, Ceram. Int. 45 (17) (2019) 21062–21076.
[2] M.S. Balogun, Y. Huang, W. Qiu, H. Yang, H. Ji, Y. Tong, Updates on the development of nanostructured transition metal nitrides for electrochemical energy storage and water splitting, Mater. Today 20 (2017) 425–451, https://doi.org/10.1016/j.mattod.2017.03.019.
[3] H. Li, T. Lv, H. Sun, G. Qian, N. Li, Y. Yao, T. Chen, Ultrastretchable and superior healable supercapacitors based on a double cross-linked hydrogel electrolyte, Nat. Commun. 10 (2019) 536, https://doi.org/10.1038/s41467-019-08320-z.
[4] C. Cao, Y. Zhou, S. Ubnoske, J. Zang, Y. Cao, P. Henry, C.B. Parker, J.T. Glass, Highly Stretchable Supercapacitors via Crumpled Vertically Aligned Carbon Nanotube Forests, Adv. Energy Mater. 9 (2019) 1900618, https://doi.org/10.1002/aenm.201900618.
[5] G. Wang, H. Wang, X. Lu, Y. Ling, M. Yu, T. Zhai, Y. Tong, Y. Li, Solid-State Supercapacitor Based on Activated Carbon Cloths Exhibits Excellent Rate Capability, Adv. Mater. 26 (2014) 2676–2682, https://doi.org/10.1002/adma.201304756.
[6] Z. Fan, Y. Wang, Z. Xie, D. Wang, Y. Yuan, H. Kang, B. Su, Z. Cheng, Y. Liu, Modified MXene/Holey Graphene Films for Advanced Supercapacitor Electrodes with Superior Energy Storage, Adv Sci (Weinh) 5 (2018) 1800750, https://doi.org/10.1002/advs.201800750.
[7] Y. Tan, L. Meng, Y. Wang, W. Dong, L. Kong, L. Kang, F. Ran, Negative electrode materials of molybdenum nitride/N-doped carbon nano-fiber via electrospinning method for high-performance supercapacitors, Electrochim. Acta 277 (2018) 41–49, https://doi.org/10.1016/j.electacta.2018.04.214.
[8] A. Dang, Y. Sun, C. Fang, T. Li, X. Liu, Y. Xia, F. Ye, A. Zada, M. Khan, Rational design of Ti3C2/carbon nanotubes/MnCo2S4 electrodes for symmetric supercapacitors with high energy storage, Appl. Surf. Sci. 581 (2022), https://doi.org/10.1016/j.apsusc.2022.152432 152432.
[9] A.G. El-Deen, M.K. Abdel-Sattar, N.K. Allam, High-performance solid-state supercapacitor based on Ni-Co layered double hydroxide@Co3O4 nanocubes

and spongy graphene electrodes, Appl. Surf. Sci. 587 (2022), https://doi.org/10.1016/j.apsusc.2022.152548 152548.
[10] R.S. Kate, S.A. Khalate, R.J. Deokate, Overview of nanostructured metal oxides and pure nickel oxide (NiO) electrodes for supercapacitors: A review, J. Power Sources 734 (2018) 89–111, https://doi.org/10.1016/j.jallcom.2017.10.262.
[11] V.S. Sumana, Y.N. Sudhakar, A. Varghese, G.K. Nagaraja, Pt nanoflower-poly (aniline) electrode material with the synchronized concept of energy storage in supercapacitor, Appl. Surf. Sci. 589 (2022), https://doi.org/10.1016/j.apsusc.2022.152994 152994.
[12] K.C. Seetha Lakshmi, X. Ji, L.-D. Shao, B. Vedhanarayanan, T.-W. Lin, Tailor-made organic polymers towards high voltage aqueous ammonium/potassium-ion asymmetric supercapacitors, Appl. Surf. Sci. 577 (2022), https://doi.org/10.1016/j.apsusc.2021.151918 151918.
[13] M.R. Pallavolu, Y. Anil Kumar, R.R. Nallapureddy, H.R. Goli, A. Narayan Banerjee, S.W. Joo, In-situ design of porous vanadium nitride@carbon nanobelts: A promising material for high-performance asymmetric supercapacitors, Appl. Surf. Sci. 575 (2022), https://doi.org/10.1016/j.apsusc.2021.151734 151734.
[14] S. Yuan, S.-Y. Pang, J. Hao, 2D transition metal dichalcogenides, carbides, nitrides, and their applications in supercapacitors and electrocatalytic hydrogen evolution reaction, Appl. Phys. Rev. 7 (2) (2020) 021304.
[15] M.S. Balogun, W. Qiu, W. Wang, P. Fang, X. Lu, Y. Tong, Recent advances in metal nitrides as high-performance electrode materials for energy storage devices, J. Mater. Chem. A 3 (2015) 1364–1387, https://doi.org/10.1039/C4TA05565A.
[16] B. Wei, H. Liang, D. Zhang, Z. Qi, H. Shen, Z. Wang, Magnetron sputtered TiN thin films toward enhanced performance supercapacitor electrodes, Mater. Renewable Sustainable Energy 7 (2018) 11, https://doi.org/10.1007/s40243-018-0117-9.
[17] B. Wei, H. Liang, D. Zhang, Z. Wu, Z. Qi, Z. Wang, CrN thin films prepared by reactive DC magnetron sputtering for symmetric supercapacitors, J. Mater. Chem. A 5 (2017) 2844–2851, https://doi.org/10.1039/c6ta09985h.
[18] B. Wei, G. Mei, H. Liang, Z. Qi, D. Zhang, H. Shen, Z. Wang, Porous CrN thin films by selectively etching CrCuN for symmetric supercapacitors, J. Power Sources 385 (2018) 39–44, https://doi.org/10.1016/j.jpowsour.2018.03.023.
[19] M. Arif, A. Sanger, A. Singh, Sputter deposited chromium nitride thin electrodes for supercapacitor applications, Mater. Lett. 220 (2018) 213–217, https://doi.org/10.1016/j.matlet.2018.02.094.
[20] R. Lucio-Porto, S. Bouhtiyya, J.F. Pierson, A. Morel, F. Capon, P. Boulet, T. Brousse, VN thin films as electrode materials for electrochemical capacitors, Electrochim. Acta 141 (2014) 203–211, https://doi.org/10.1016/j.electacta.2014.07.056.
[21] Z. Gao, Z. Wu, S. Zhao, T. Zhang, Q. Wang, Enhanced capacitive property of HfN film electrode by plasma etching for supercapacitors, Mater. Lett. 235 (2019) 148–152, https://doi.org/10.1016/j.matlet.2018.10.032.
[22] B. Ranjan, G.K. Sharma, D. Kaur, Rationally synthesized Mo2N nanopyramids for high-performance flexible supercapacitive electrodes with deep insight into the Na-ion storage mechanism, Appl. Surf. Sci. 588 (2022), https://doi.org/10.1016/j.apsusc.2022.152925 152925.
[23] Y. Xu, L. Chen, Z. Liu, F. Pei, Y. Du, Influence of Ti on the mechanical properties, thermal stability and oxidation resistance of Al-Cr-N coatings, Vacuum 120 (2015) 127–131, https://doi.org/10.1016/j.vacuum.2015.07.004.
[24] A. Achour, M. Islam, I. Ahmad, L. Le Brizoual, A. Djouadi, T. Brousse, Influence of surface chemistry and point defects in TiN based electrodes on electrochemical capacitive storage activity, Scr. Mater. 153 (2018) 59–62, https://doi.org/10.1016/j.scriptamat.2018.04.051.
[25] Z. Gao, Z. Wan, Z. Wu, X. Huang, H. Li, T.F. Zhang, P.H. Mayrhofer, Q. Wang, Synthesis and electrochemical properties of nanoporous CrN thin film electrodes for supercapacitor applications, Mater. Des. 209 (2021), https://doi.org/10.1016/j.matdes.2021.109949 109949.
[26] K. Robbie, M.J. Brett, Sculptured thin films and glancing angle deposition: Growth mechanics and applications, J. Vac. Sci. Technol., A 15 (1997) 1460–1465, https://doi.org/10.1116/1.580562.
[27] Z. Qi, B. Wei, J. Wang, Y. Yang, Z. Wang, Nanostructured porous CrN thin films by oblique angle magnetron sputtering for symmetric supercapacitors, J. Power Sources 806 (2019) 953–959, https://doi.org/10.1016/j.jallcom.2019.07.325.
[28] S.H. Kim, S.H. Lee, J.S. Yu, Broadband and antireflective characteristics of glancing angle deposited titanium dioxide nanostructures for photovoltaic applications, Thin Solid Films 685 (2019) 53–58, https://doi.org/10.1016/j.tsf.2019.05.067.
[29] M.J. Cordill, T. Jörg, O. Glushko, R. Franz, C. Mitterer, Crack deflecting microstructure for improved electro-mechanical lifetimes of flexible systems, Mater. Lett. 244 (2019) 47–49, https://doi.org/10.1016/j.matlet.2019.02.039.
[30] E. Haye, A. Achour, A. Guerra, F. Moulaï, T. Hadjersi, R. Boukherroub, A. Panepinto, T. Brousse, J.-J. Pireaux, S. Lucas, Achieving on chip micro-supercapacitors based on CrN deposited by bipolar magnetron sputtering at glancing angle, Electrochim. Acta 324 (2019), https://doi.org/10.1016/j.electacta.2019.134890 134890.
[31] W. Tillmann, D. Kokalj, D. Stangier, Influence of the deposition parameters on the texture and mechanical properties of magnetron sputtered cubic MoNx thin films, Materialia 5 (2019), https://doi.org/10.1016/j.mtla.2018.100186 100186.
[32] J. Qian, S. Li, J. Pu, Z. Cai, H. Wang, Q. Cai, P. Ju, Effect of heat treatment on structure and properties of molybdenum nitride and molybdenum carbonitride films prepared by magnetron sputtering, Surf. Coat. Technol. 374 (2019) 725–735, https://doi.org/10.1016/j.surfcoat.2019.06.062.
[33] T. Wang, J. Zhang, Y. Li, F. Gao, G. Zhang, Self-lubricating TiN/MoN and TiAlN/MoN nano-multilayer coatings for drilling of austenitic stainless steel, Ceram. Int. 45 (2019) 24248–24253, https://doi.org/10.1016/j.ceramint.2019.08.136.
[34] G. Ma, Z. Wang, B. Gao, T. Ding, Q. Zhong, X. Peng, J. Su, B. Hu, L. Yuan, P.K. Chu, J. Zhou, K. Huo, Multilayered paper-like electrodes composed of alternating stacked mesoporous Mo2N nanobelts and reduced graphene oxide for flexible all-solid-state supercapacitors, J. Mater. Chem. A 3 (2015) 14617–14624, https://doi.org/10.1039/C5TA02851E.
[35] L. Liu, B. Shen, D. Jiang, R. Guo, L. Kong, X. Yan, Watchband-Like Supercapacitors with Body Temperature Inducible Shape Memory Ability, Adv. Energy Mater. 6 (2016) 1600763, https://doi.org/10.1002/aenm.201600763.
[36] J. Dervaux, P.A. Cormier, P. Moskovkin, O. Douheret, S. Konstantinidis, R. Lazzaroni, S. Lucas, R. Snyders, Synthesis of nanostructured Ti thin films by combining glancing angle deposition and magnetron sputtering: A joint experimental and modeling study, Thin Solid Films 636 (2017) 644–657, https://doi.org/10.1016/j.tsf.2017.06.006.
[37] A. Gomathi, A. Sundaresan, C.N.R. Rao, Nanoparticles of superconducting γ-Mo2N and δ-MoN, J. Solid State Chem. 180 (2007) 291–295, https://doi.org/10.1016/j.jssc.2006.10.020.
[38] H. Jehn, P. Ettmayer, The molybdenum-nitrogen phase diagram, Journal of the Less Common Metals 58 (1978) 85–98, https://doi.org/10.1016/0022-5088(78)90073-5.
[39] Y. Xie, F. Tian, Capacitive performance of molybdenum nitride/titanium nitride nanotube array for supercapacitor, Mater. Sci. Eng. B 215 (2017) 64–70, https://doi.org/10.1016/j.mseb.2016.11.005.
[40] K. Robert, D. Stiévenard, D. Deresmes, C. Douard, A. Iadecola, D. Troadec, P. Simon, N. Nuns, M. Marinova, M. Huvé, P. Roussel, T. Brousse, C. Lethien, Novel insights into the charge storage mechanism in pseudocapacitive vanadium nitride thick films for high-performance on-chip micro-supercapacitors, Energ. Environ. Sci. 13 (2020) 949–957, https://doi.org/10.1039/C9EE03787J.
[41] P. Pande, P.G. Rasmussen, L.T. Thompson, Charge storage on nanostructured early transition metal nitrides and carbides, J. Power Sources 207 (2012) 212–215, https://doi.org/10.1016/j.jpowsour.2012.01.028.
[42] J. Chen, K. Sheng, P. Luo, C. Li, G. Shi, Graphene Hydrogels Deposited in Nickel Foams for High-Rate Electrochemical Capacitors, Adv. Mater. 24 (2012) 4569–4573, https://doi.org/10.1002/adma.201201978.
[43] Y.X. Xu, L. Chen, F. Pei, K.K. Chang, Y. Du, Effect of the modulation ratio on the interface structure of TiAlN/TiN and TiAlN/ZrN multilayers: First-principles and experimental investigations, Acta Mater. 130 (2017) 281–288, https://doi.org/10.1016/j.actamat.2017.03.053.
[44] Q. Akbar Sial, L. Thai Duy, R. Singh, S. Iqbal, R. Yeasmin, Y.-J. Lee, S.S. Kalanur, H. Seo, A multifunctional TiN/Ni electrode for wearable supercapacitor and sensor with an insight into charge storage mechanism, Appl. Surf. Sci. 555 (2021), https://doi.org/10.1016/j.apsusc.2021.149718 149718.
[45] L. Chen, C. Liu, Z. Zhang, Novel (111) oriented γ-Mo_2N thin films deposited by magnetron sputtering as an anode for aqueous micro-supercapacitors, Electrochim. Acta 245 (2017) 237–248, https://doi.org/10.1016/j.electacta.2017.05.102.
[46] X. Hou, Q. Li, L. Zhang, T. Yang, J. Chen, L. Su, Tunable preparation of chrysanthemum-like titanium nitride as flexible electrode materials for ultrafast-charging/discharging and excellent stable supercapacitors, J. Power Sources 396 (2018) 319–326, https://doi.org/10.1016/j.jpowsour.2018.06.033.
[47] L. Du, P. Yang, X. Yu, P. Liu, J. Song, W. Mai, Flexible supercapacitors based on carbon nanotube/MnO2 nanotube hybrid porous films for wearable electronic devices, J. Mater. Chem. A 2 (2014) 17561–17567, https://doi.org/10.1039/C4TA04431B.
[48] P. Yang, Y. Chen, X. Yu, P. Qiang, K. Wang, X. Cai, S. Tan, P. Liu, J. Song, W. Mai, Reciprocal alternate deposition strategy using metal oxide/carbon nanotube for positive and negative electrodes of high-performance supercapacitors, Nano Energy 10 (2014) 108–116, https://doi.org/10.1016/j.nanoen.2014.08.018.